

The High Time Resolution Universe Pulsar Survey – VII: discovery of five millisecond pulsars and the different luminosity properties of binary and isolated recycled pulsars.

M. Burgay^{1*}, M. Bailes^{2,3}, S. D. Bates⁴, N. D. R. Bhat^{2,5}, S. Burke-Spolaor⁶,
D. J. Champion⁷, P. Coster^{2,8}, N. D’Amico^{1,9}, S. Johnston⁸, M. J. Keith⁸, M. Kramer^{7,10},
L. Levin⁴, A. G. Lyne¹⁰, S. Milia¹, C. Ng⁷, A. Possenti¹, B. W. Stappers¹⁰, D. Thornton^{10,8},
C. Tiburzi^{1,9}, W. van Straten², C. G. Bassa¹⁰

¹INAF/Osservatorio Astronomico di Cagliari, località Poggio dei Pini, strada 54, 09012 Capoterra, Italy

²Centre for Astrophysics and Supercomputing, Swinburne University of Technology, Mail H39, PO Box 218, VIC 3122, Australia

³ARC Centre of Excellence for All-sky Astrophysics, 44 Rosehill Street Redfern, NSW 2016, Australia

⁴Department of Physics, West Virginia University, 111 Hodges Hall, PO Box 6315, Morgantown, WV 26506, USA

⁵International Centre for Radio Astronomy Research, Curtin University, Bentley, WA 6102, Australia

⁶Jet Propulsion Laboratory, California Institute of Technology, 4800 Oak Grove Drive, Pasadena CA 91104 USA

⁷Max Planck Institut für Radioastronomie, Auf dem Hügel 69, 53121 Bonn, Germany

⁸CSIRO Astronomy and Space Science, Australia Telescope National Facility, PO Box 76, Epping, NSW 1710, Australia

⁹Dipartimento di Fisica, Università degli Studi di Cagliari, SP Monserrato-Sestu km 0.7, I-09042 Monserrato, Italy

¹⁰Jodrell Bank Centre for Astrophysics, University of Manchester, Alan Turing Building, Oxford Road, Manchester M13 9PL, United Kingdom

ABSTRACT

This paper presents the discovery and timing parameters for five millisecond pulsars (MSPs), four in binary systems with probable white dwarf companions and one isolated, found in ongoing processing of the High Time Resolution Universe Pulsar Survey (HTRU). We also present high quality polarimetric data on four of them. These further discoveries confirm the high potential of our survey in finding pulsars with very short spin periods. At least two of these five MSPs are excellent candidates to be included in the Pulsar Timing Array projects. Thanks to the wealth of MSP discoveries in the HTRU survey, we revisit the question of whether the luminosity distributions of isolated and binary MSPs are different. Using the Cordes and Lazio distance model and our new and catalogue flux density measurements, we find that 41 of the 42 most luminous MSPs in the Galactic disk are in binaries and a statistical analysis suggests that the luminosity functions differ with 99.9% significance. We conclude that the formation process that leads to solitary MSPs affects their luminosities, despite their period and period derivatives being similar to those of pulsars in binary systems.

Key words: stars: pulsars: individual: PSR J1431–5740, PSR J1545–4550, PSR J1825–0319, PSR J1832–0836, PSR J2236–5527

1 INTRODUCTION

According to the *recycling* model (e.g. Alpar et al. 1982) millisecond - or recycled - pulsars (MSPs) are formed in binary systems where the companion star transfers mass, and hence angular momentum, onto the neutron star (NS). Extended mass transfer from low mass companions can cause the NS to be spun up to rotational periods of at least 1.5 milliseconds. Higher mass systems, transferring mass over shorter time scales and mostly via a wind (Bhattacharya & van den Heuvel 1991), cannot push the recycling

process down to periods below ~ 20 milliseconds. At the same time, due to still unclear mechanisms, possibly linked to the accreted mass itself, the magnetic field B is decreased down to 10^{8-10} G.

About 75% of all known MSPs in the Galactic field (i.e. outside Globular Clusters, where exchange interactions can change the final outcome of the evolution of an MSP) are found in binary systems (data from the ATNF pulsar catalogue¹; Manchester et al. 2005), supporting the above scenario. The formation path of isolated MSPs, though, is still a matter of debate: those with

* E-mail:burgay@oa-cagliari.inaf.it

¹ <http://www.atnf.csiro.au/people/pulsar/psrcat/>

spin periods of few tens of ms or more could derive from double neutron star systems disrupted during the second supernova explosion (Disrupted Recycled Pulsars, DRPs; Camilo et al. 1996; Lorimer et al. 2004) while the shorter period pulsars could be the result of a binary system where the companion was so light that the interaction with the pulsar wind was able to completely destroy it (Bhattacharya & van den Heuvel 1991). There are now a few examples of the so called *black widow* (BW) pulsar systems (Kluźniak et al. 1988; Phinney et al. 1988; van den Heuvel & van Paradijs 1988), in which the companion star is very light and in which the radio signal is eclipsed by matter ablated from the companion for significant parts of the orbit. These objects have been suggested as possible progenitors of the shorter period isolated MSPs, although the ablation time scales seem to be generally too long for this process (Stappers et al. 1996). Until recently very few BW pulsars were known in the Galactic field. The situation has changed in the last few years thanks to deep radio follow-ups of gamma-ray point sources detected by the LAT (Atwood et al. 2009) instrument on board the *Fermi* satellite (see e.g. Ray et al. 2012 and references therein), through which also binary pulsars whose radio signal was eclipsed for a large fraction of the orbit were discovered. We note that, in average black widows detected through this channel are more energetic, show longer eclipses and have lighter companions than those previously known, hence it is likely that the mass loss rate is higher and the time for complete ablation of their companions shorter.

Other possible explanations of the formation of isolated MSPs invoke different paths: one example is the accretion-induced collapse of a white dwarf (Bailyn & Grindlay 1990), another is white dwarf mergers (Michel 1987). Finding intrinsic differences between the two MSP populations might point to a different origin and/or evolutionary path for the isolated MSPs.

MSPs are more stable clocks than the non-recycled pulsars (PSRs). When in binary systems, their stable rotation allows precise determination of the Keplerian orbital parameters and, in some cases, also the post-Keplerian parameters, making these pulsars laboratories for testing relativistic gravity in the strong field regime (e.g. Stairs et al. 2002; Kramer et al. 2006; Weisberg et al. 2010). If the rotational stability and timing precision are high enough, MSPs can be used in timing arrays for gravitational wave detection (Hellings & Downs 1983).

The High Time Resolution Universe survey (HTRU; Keith et al. 2010), whose observations started at the Parkes observatory (NSW, Australia) in 2008, was primarily designed to discover MSPs missed in previous surveys. Thanks to the new digital backends adopted in this experiment, the time and frequency resolutions have improved by a factor of 4 and 8 respectively. This allows the survey to sample a much larger volume of the Galaxy for short period pulsars as the deleterious effects of dispersion are greatly diminished. The suitability of the chosen parameters of the survey to discover MSPs has been already demonstrated in Bates et al. (2011) where we presented the first five new objects of this class found in the intermediate latitude ($|b| < 15^\circ$) part of the survey. In this paper we present the discovery and timing parameters of five further such objects, confirming the very high potential of our acquisition system.

In section §2 we briefly describe the follow-up observations and report the spin, orbital and astrometric parameters resulting from the timing campaign on the five discovered MSPs, highlighting their potential as ‘test particles’ in the timing array experiments. Given the increased sample of recycled pulsars, in §3 we revise the luminosity distribution of isolated versus binary MSPs and find

them to be very different. In §4 we briefly report on the search for gamma-ray counterparts to our discoveries. Finally, in §5 we describe the polarimetric characteristics for four of the new discoveries.

2 OBSERVATIONS AND TIMING ANALYSIS

Of the five newly discovered MSPs, four were found in the data of the intermediate latitude part of the HTRU survey, consisting of 540s pointings covering the area enclosed by Galactic coordinates $-120^\circ < l < 30^\circ$, $|b| < 15^\circ$. The fifth, J2236–5527, was discovered in the high latitude part of the survey: 270s pointings covering the entire southern sky below declination $+10^\circ$ (except the intermediate latitude part mentioned above).

When a pulsar is discovered only its approximate spin period, dispersion measure (DM, i.e. the free electron column density along the line of sight) and position are known. To ensure that the full potential of these discoveries is exploited, a precise determination of the pulsars’ position is needed (e.g. to look for counterparts at other wavelengths; see §4) and accurate measurements of the spin, astrometric, and if they belong to a binary system, orbital parameters are necessary. To obtain these parameters one has to start a follow-up timing campaign covering a time span of at least one year.

For the HTRU MSPs, confirmations, gridding observations (aimed at determining a more precise position for the pulsar with a grid of 5 adjacent pointings; Morris et al. 2002) and the first timing observations, are done with the same instrumentation used for the survey pointings (see Keith et al. 2010). This allows the raw data to be retained with all the time samples and the frequency channels, in such a way as to be able to recover the periodic signal even if the apparent spin period is significantly different from the discovery one because of orbital motion. The rest of the timing observations, done with an approximately monthly cadence, are performed either with the Parkes 64-m telescope or, for the objects visible from the Northern hemisphere, with the Lovell Telescope (Jodrell Bank, Manchester, UK). At both sites an ATNF digital filterbank (DFB) is used as backend and most of the observations are performed at a wavelength close to 20 cm. In particular, at the Parkes telescope the data are acquired over 256 MHz of bandwidth centered at a frequency of 1369 MHz and split into 1024 frequency channels, while the Lovell data cover a frequency range of 384 MHz centred at 1532 MHz and split into 1024 frequency channels, more than 1/4 of which, until September 2012, were removed through a band-pass filter because of Radio Frequency Interferences (RFI). After that date the Lovell data have been manually cleaned from RFI and a larger part of the band has been used. DFB data are folded on-line using the pulsar ephemeris obtained from the first stages of timing and refined as the follow-up observations proceed. Observations of PSR J1832–0836 at Jodrell Bank were performed also using the *ROACH* pulsar backend. This backend uses a *ROACH* FPGA board² to perform either baseband recording or coherent dedispersion of two 8-bit Nyquist sampled orthogonal polarisations over a total bandwidth of 512 MHz. After sampling and digitization, the *ROACH* board channelizes the signal into 32 sub-bands of 16 MHz, each of which is coherently dedispersed and folded using an 8-core Intel Xeon computer running the *dspsr* software package (van Straten & Bailes 2011). As the total usable bandwidth of

² <https://casper.berkeley.edu/wiki/ROACH>

the L-band receiver is 400 MHz, the data from 25 subbands is combined and analyzed with the `psrchive` package³ (Hotan et al. 2004). Also in this case about 1/4 of the bandwidth was removed because of RFI until September 2012. After about one year of timing observations the covariance in the timing parameters is broken and a precise timing solution is obtained. Times of arrival are obtained using `pat` from `psrchive` through cross-correlation with an analytic profile template created by fitting von Mises functions to profile components.

Table 1 reports the main detection characteristics of the five newly discovered pulsars: for each object the timing position in Galactic coordinates, the beam in which the pulsar was detected, the radial distance of the pulsar from the discovery beam centre in units of the beam radius, the signal-to-noise ratio (S/N) of the discovery observation, the mean flux density S and the pulse widths at 50% and 10% of the peak of the mean pulse profile are listed. For the three pulsars timed at the Parkes observatory, the values of the fluxes are properly calibrated on a reference source (see §5). For polarisation measurement purposes (see §5) J1832–0836, timed over more than one year with the Lovell telescope, was also observed on one occasion for ~ 1.5 hrs with the Parkes Radio Telescope and hence as also properly flux calibrated. The flux density value for the remaining pulsar has been obtained using the radiometer equation (see e.g. Manchester et al. 2001) scaled using the calibrated flux densities of the other four MSPs. For J1545–4550, for which we have a flux measurement also at 10 cm and 40 cm, we could calculate a spectral index α (with $S \propto \nu^{-\alpha}$) of 1.15 ± 0.09 for the main peak, and a steeper, though less constrained, spectral index of 2.0 ± 0.6 for the second peak.

2.1 Binary pulsars

Four of the five newly discovered pulsars orbit companions with minimum masses ranging from $0.15 M_{\odot}$ to $0.22 M_{\odot}$ (see Table 2). This mass range suggests that the companion stars are Helium white dwarfs (He-WD), a hypothesis supported by the fact that their measured orbital periods and eccentricities (Tab. 2) nicely follow the orbital relation predicted by Phinney (1992) for Low Mass Binary Pulsars with He-WDs companions (see Figure 1).

The ephemerides resulting from the timing campaign of the binary MSPs J1431–5740, J1545–4550, J1825–0319 and J2236–5527 are obtained with `tempo2` (Hobbs et al. 2006) and are presented in Table 2. In the cases of J1545–4550 and J2236–5527, polarisation calibration (see §5) allowed to further improve the rms of the residuals of the timing solution with respect to that obtained using uncalibrated data, by 5% and 12% respectively. We note that, here and in Table 3, the values for \dot{P} (and the parameters derived from it) are not corrected for the contributions of the acceleration along the line of sight due to the potential well of the Galaxy and of the unknown transverse velocity of the pulsar (Shklovskii 1970). Even though our current data span is not long enough to measure a proper motion, if we assume an average velocity of 70 km/s (Hobbs et al. 2005), we obtain contributions to the measured \dot{P} s of 2 to 18 per cent, depending on the source. The uncertainty in the distances to the pulsars also contributes to the uncertainty in the intrinsic value of the spin-down. The listed values of the spin period derivative and of the derived quantities should hence be taken as upper limits (lower limits, in the case of the age).

The timing residuals for J1545–4550 have an rms smaller

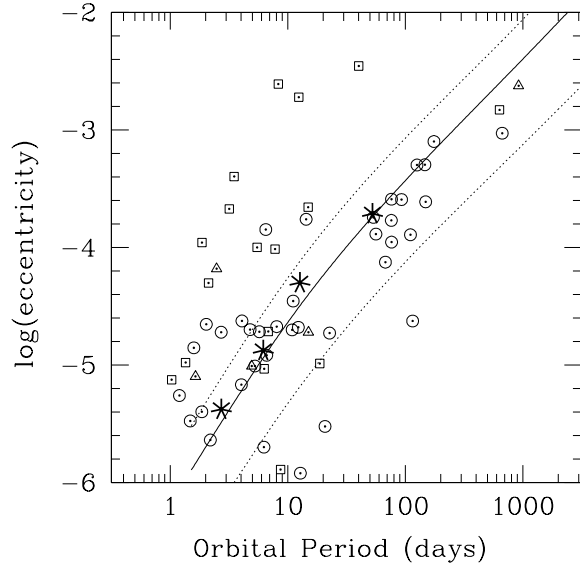


Figure 1. Orbital eccentricity vs orbital period of binary pulsars in the disk of the Galaxy with measured eccentricities $e < 0.1$ (data taken from the ATNF pulsar catalogue; Manchester et al. 2005). The dotted lines contain 95% of the eccentricities of He-WD MSPs according to the model of Phinney & Kulkarni (1994). The binary pulsars from this work are represented by black asterisks. Squares are Intermediate Mass Binary Pulsars and circles are Low Mass Binary Pulsars, while triangles denote pulsars not falling in these categories (e.g. the HTRU Very Low Mass Binary pulsar J1502–6752, Keith et al. 2012) or whose classification is still uncertain (Camilo et al. 2001; Edwards & Bailes 2001; Lorimer et al. 2006; Janssen et al. 2010; Keith et al. 2012).

than $1 \mu\text{s}$, demonstrating why this pulsar has, as of March 2012, been included in the Parkes Pulsar Timing Array (PPTA; e.g. Coles et al. 2013) for the detection of stochastic gravitational wave background. PPTA observations are performed at intervals of 2 - 3 weeks in three frequency bands: besides the 20-cm dataset collected starting in May 2011, for J1545–4550 we hence also have a small number of 10-cm and 40-cm observations (central frequencies of 3100 and 732 MHz respectively and bandwidths of 1024 and 64 MHz respectively, split into 1024 channels). Profiles at the three frequencies are shown in Fig. 4.

2.2 The isolated MSP J1832–0836

Timing results from 1.3 years of follow-up observations of the isolated MSP J1832–0836 with the Lovell telescope are presented in Table 3. As for the binary MSPs, the \dot{P} value is not corrected for the contributions of the acceleration along the line of sight due to the potential well of the Galaxy and of the transverse velocity of the pulsar.

The residuals of this pulsar have the third-smallest rms ($2.0 \mu\text{s}$; see Tab. 3) among the HTRU MSPs discovered so far. This target is hence another good candidate for Timing Array studies and may be included in the target list for the European and North American Pulsar Timing Arrays (EPTA; Ferdman et al. 2010 and NANOGrav; Jenet et al. 2009), also considering that the current results are likely to be improved, having been obtained with relatively short timing observations (20 minutes or less over a clean bandwidth of $\lesssim 300$ MHz) and with no polarisation calibration.

³ <http://psrchive.sourceforge.net/>

Table 1. From left to right, we report, for our 5 MSPs, the name, the Galactic coordinates obtained from timing, offset with respect to the discovery position in beam radii, signal-to-noise ratio at discovery, mean flux density and pulse widths measured at 10% and 50% of the peak. For the pulsars with multiple profiles the pulse widths refer to the main peak alone. For J1545–4550 we report the flux density S and pulse widths values at 10 cm^a and 40 cm^b as well. All the other numbers refer to the 20-cm observations. The numbers in parentheses are the 2- σ errors on the last quoted digit(s). A 30% error on the flux density is assumed for the uncalibrated measurement.

Name	l ($^{\circ}$)	b ($^{\circ}$)	Δ_{pos}	beam (beam radii)	S/N	S (mJy)	W_{10} (ms)	W_{50} (ms)
J1431–5740	315.96	2.66	0.47	11	10.9	0.351(8)	0.482	0.176
J1545–4550	331.89	6.99	0.69	10	16.6	0.752(6)	0.299	0.128
J1545–4550 ^a			–	–	–	0.209(6)	0.242	0.084
J1545–4550 ^b			–	–	–	1.94(4)	0.746	0.284
J1825–0319	27.05	4.14	0.38	12	11.1	0.20(6)	0.385	0.149
J1832–0836	23.11	0.26	0.43	9	13.9	1.10(2)	0.339	0.058
J2236–5527	334.17	–52.72	0.67	1	27.8	0.282(8)	0.979	0.195

Table 2. Timing parameters for the four binary pulsars discovered. In the top section of the table the measured astrometric, rotational and orbital parameters are listed: J2000 right ascension and declination obtained with the DE405 solar system ephemeris, spin period, period derivative, reference epoch for the spin period, dispersion measure, orbital period, projected semi-major axis, epoch of periastron, orbital eccentricity and longitude of periastron. The ELL1 binary model (Wex 1998) was used to fit such low eccentricities and the values reported have been derived from the EPS1, EPS2 and TASC parameters given by the model. The second part reports the derived parameters: minimum companion mass, implied dipolar magnetic field strength, characteristic age, spin-down energy, distance as derived from the DM and the NE2001 model (Cordes & Lazio 2002) for the distribution of free electrons in the Galaxy, and the luminosity at 20 cm (calculated as $S \times \text{Dist}^2$). The last part lists the time span covered by the timing data, the final timing solution rms residuals, the factor EFAC for which the times of arrival were multiplied to obtain a reduced χ^2 of 1 and the number of times of arrival used. Numbers in parentheses are twice the formal tempo2 errors on the last quoted digit(s). To obtain these ephemerides, as well as those in table 3 the Barycentric Coordinate Time TCB, the standard for tempo2 , was used.

	J1431–5740	J1545–4550	J1825–0319	J2236–5527
Ra (h m s)	14:31:03.4953(3)	15:45:55.94596(4)	18:25:55.9531(5)	22:36:51.8510(8)
Dec ($^{\circ}$ $'$ $''$)	–57:40:11.670(4)	–45:50:37.5272(8)	–03:19:57.570(15)	–55:27:48.833(4)
P (ms)	4.1105439567658(12)	3.57528861884712(12)	4.553527919736(4)	6.907549392921(3)
\dot{P} (s/s)	$6.42(12) \times 10^{-21}$	$5.250(3) \times 10^{-20}$	$6.8(3) \times 10^{-21}$	$9.6(6) \times 10^{-21}$
Pepoch (MJD)	55865	55937	55784	55758
DM (pc cm ^{–3})	131.46(3)	68.390(8)	119.5(4)	20.00(5)
P_b (days)	2.726855823(16)	6.203064928(8)	52.6304992(16)	12.68918715(14)
$a \sin i$ (lt-s)	2.269890(4)	3.8469053(6)	18.266400(11)	8.775877(7)
T_0 (MJD)	55461.79(27)	55611.40(2)	55805.06(5)	55472.551(7)
e	$4.3(28) \times 10^{-6}$	$1.30(4) \times 10^{-5}$	$1.939(12) \times 10^{-4}$	$5.02(18) \times 10^{-5}$
ω (deg)	95(40)	221.3(18)	93.2(4)	350.8(18)
$M_{2,\text{min}}$ (M_{\odot})	0.156	0.153	0.177	0.223
B (G)	1.64×10^8	4.38×10^8	1.78×10^8	2.61×10^8
τ_c (yr)	1.01×10^{10}	1.08×10^9	1.06×10^{10}	1.14×10^{10}
\dot{E} (erg s ^{–1})	3.6×10^{33}	4.5×10^{34}	2.9×10^{33}	1.2×10^{33}
Dist (kpc)	2.6	2.1	3.1	0.8
L_{1400} (mJy kpc ²)	2.4	3.3	1.9	0.2
Start (MJD)	55539.861	55685.428	55267.462	55504.474
Finish (MJD)	56190.182	56190.238	56159.946	56013.031
Data span (yr)	1.8	1.4	2.4	1.4
rms (μ s)	5.638	0.825	21.273	5.355
EFAC	1.021	0.7828	1.291	0.985
NTToA	45	30	61	35

This pulsar, with its 1400-MHz luminosity of 1.3 mJy kpc² (2.2 mJy kpc² if we use the distance obtained with the Taylor & Cordes 1993 electron density model), is among the brightest isolated MSPs yet discovered.

3 MSP LUMINOSITY DISTRIBUTION

Prompted by the case of J1832–0836, we briefly revise here the comparison between the luminosity of isolated and binary MSPs, taking advantage of the fact that in the recent years the number of Galactic field MSPs, both isolated and in binary systems, has increased significantly.

Lorimer et al. (2007) showed that the apparent differences in the luminosity distributions seen in isolated and binary MSPs se-

Table 3. Ephemeris for the isolated pulsar J1832–0836. The parameters are the same as in Tab. 2.

J1832–0836	
Ra (h m s)	18:32:27.59442(4)
Dec (° ′ ″)	−08:36:54.54.969(3)
P (ms)	2.7191120623197(3)
\dot{P} (s/s)	$8.62(5) \times 10^{-21}$
Pepoch (MJD)	55936
DM (pc cm ^{−3})	28.18(9)
<hr/>	
B (G)	1.55×10^8
τ_c (yr)	$5.00e \times 10^9$
\dot{E} (erg s ^{−1})	1.7×10^{34}
Dist (kpc)	1.1
L_{1400} (mJy kpc ²)	1.3
<hr/>	
Start (MJD)	55691.211
Finish (MJD)	56188.933
Data span (yr)	1.3
rms (μs)	2.0
EFAC	1.382
NToA	43

lected from the early 430-MHz surveys (Bailes et al. 1997) could be explained by small-number statistics and observational selection biases. An examination of a sample of 33 objects (11 isolated and 22 binaries) from 1400-MHz surveys showed no statistically significant differences in the distributions: the significance level of a Kolmogorov-Smirnov test (KS test; see e.g. Press et al. 1986) was a mere 70.9% (while it was 99.1% for the 430-MHz sample). Lorimer et al. (2007) concluded that there was no intrinsic difference in the two MSPs populations.

Figure 2 shows the updated distributions of the 1400 MHz luminosity for 87 Galactic binary MSPs (dotted histogram; 13 in the smaller shaded histogram are black widow pulsars, while the remaining binaries are contained in the bigger shaded region) and 18 isolated MSPs (thick line histogram). We here define MSP as all the recycled pulsars having spin period $P < 0.1$ s and surface magnetic field $B < 2 \times 10^{10}$ G. The results reported below do not significantly change even if we consider only the fully recycled MSPs with $P < 0.01$ s. The distances adopted for the calculation of the luminosities have been obtained using the NE2001 model (Cordes & Lazio 2002) for the distribution of free electrons in the Galaxy. A KS test on these two populations suggests, with 99.9% probability, that the two distributions differ. Using the distances from the Taylor & Cordes (1993) model the probability is still 98.6% and is again 99.9% if we adopt the modified version of the Taylor & Cordes (1993) model, found to more closely reproduce the distances of pulsars with measured parallaxes (Schnitzler 2012). This result is in accordance with the earlier findings by Bailes et al. (1997), Kramer et al. (1998) and Lommen et al. (2006), but in contrast with the aforementioned more recent work of Lorimer et al. (2007), which had a much smaller sample than ours. No difference in the period, period derivative nor spin-down energy is seen between the two populations (KS probabilities of 47.9%, 47.9% and 72.0% respectively, and even smaller considering fully recycled MSPs only).

One could argue that the discrepancy in luminosity can arise from the fact that, in the current analysis of HTRU data (and in some of the previous surveys), no correction for the pulsar orbital motion through acceleration searches (see e.g. Faulkner et al. 2004;

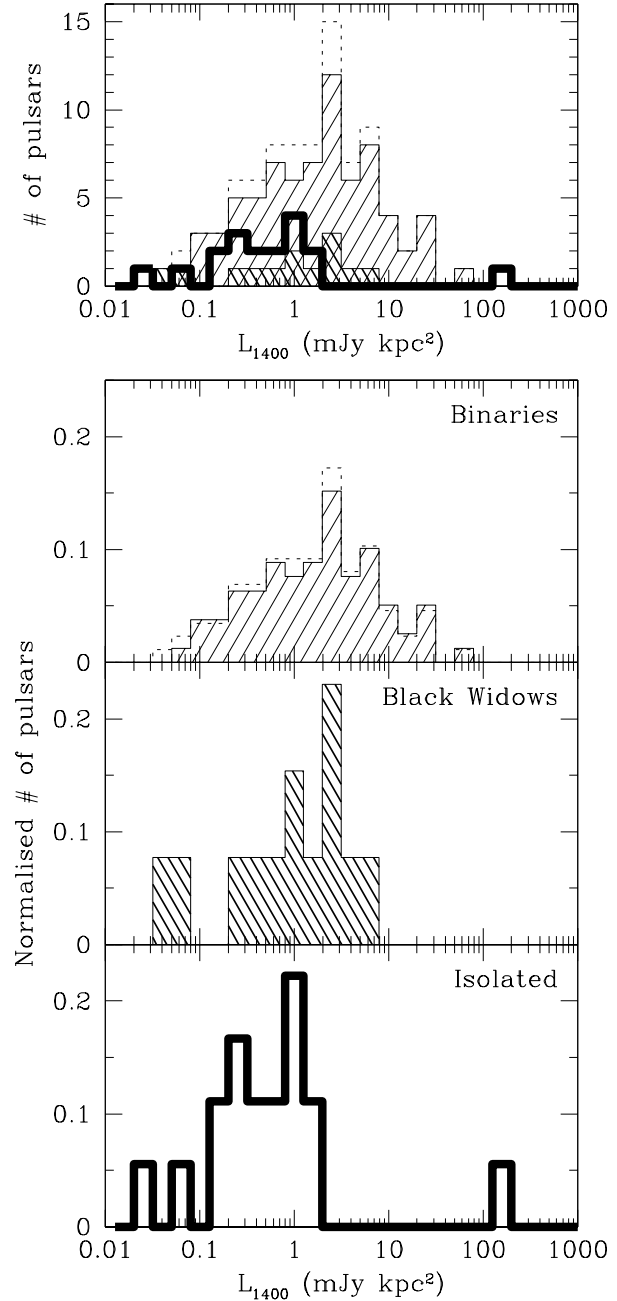


Figure 2. 1400-MHz luminosity distributions for a sample of 105 Galactic recycled pulsars. The dotted histogram shows the distribution for 87 binary MSPs, 13 of which, included in the more densely shaded histogram, belong to the class of black widow pulsars. The less densely shaded histogram contains the other binaries. The thick line shows the distribution for 18 isolated MSPs. In the top panel all the MSP populations are shown unscaled. In the bottom three panels binaries, black widows and isolated distributions have been normalised to the total number of pulsars of each type. Flux densities at 1400-MHz are taken from the ATNF pulsar catalogue (Manchester et al. 2005), Thornton et al (in preparation) and this paper. For six black widows flux densities (scaled at 1400-MHz with a spectral index $\alpha = 1.8$) are taken from Hessels et al. (2011), Ransom et al. (2011), Roy et al. (2012) and Ray et al. (2013). The luminosities are computed using the distance from the NE2001 model (Cordes & Lazio 2002).

Ransom et al. 2002; Eatough et al. 2013) has been done, leading to a loss of faint tight binaries in the sample used. This could have enhanced the discrepancy in luminosity between binary and isolated MSPs. However, if we restrict our analysis to binary MSPs with orbital periods greater than 1 day, easily detectable without any acceleration search in our 9 minutes observations, we end up with a sample of 65 binaries whose luminosity distribution still differs from that of isolated MSP with a probability of 99.9%, confirming our previous statement. We note also that the residual observational bias that could be affecting the detection of tighter system will be overcome in the near future: acceleration searches of the HTRU data are in fact under way for the low-latitude section of the survey (Ng et al. in preparation) and are about to be performed, with the use of GPUs, on the entire mid-latitude section.

We therefore claim that the intrinsic luminosity functions are indeed different, and may reflect differences in the evolutionary history of isolated and binary MSPs. In the framework of the recycling scenario, for instance, the progenitors of binary MSPs and isolated MSPs could have experienced different kinds of accretion phases (this is certainly true for the DRPs – only 3 in our sample – which are subjected to a smaller amount of mass transfer), as also speculated by Kramer et al. (1998). In particular, if isolated MSPs are the final outcome of black widow pulsars that completely ablate their companions (we hence exclude DRPs in this case), we could imagine that, during the mass transfer in the ultracompact low-mass X-ray binary leading to the BW formation, some modification is left in their magnetosphere which is later reflected on their radio luminosity.

If this was the case we would expect the luminosity distribution of BWs to be close to that of isolated MSPs and to differ from that of pulsars in other binary systems. A KS test comparing the 1400-MHz luminosity of our sample of binaries (excluding BWs) with that of 13 black widow pulsars (smaller, more densely shaded histogram in Fig. 2) gives, however, a probability of only 59.8% that the two distributions derive from different populations (the probability goes up to 87.7% if we compare BWs to isolated MSPs). We note however that, besides the small number statistics and the errors introduced in the luminosity calculation by the poor knowledge of the distances, in the case of the BW sample there is an additional uncertainty affecting the results: about a half of the flux densities reported in the literature (Hessels et al. 2011; Ransom et al. 2011; Roy et al. 2012; Ray et al. 2013), in fact, have been measured at a frequency other than 1400-MHz and have been scaled to 1400-MHz using a theoretical spectral index $\alpha = 1.8$.

If, as the above considerations seem to suggest, the details of the accretion phases are hardly responsible for the differences in luminosity, another possibility, continuing with the assumption that isolated MSPs derive from BWs, is that the time span necessary to achieve the complete ablation of the companion is very long and consequently the population of isolated MSPs should be entirely made of old objects (on average older than the BWs), while the rest of the binaries should cover a wider span of ages, from the younger more luminous ones to the older ones with luminosities similar to those of the isolated MSPs. A correlation between luminosity and age might hence exist. We note however that such a correlation is extremely difficult (if not impossible) to be properly tested, given that the characteristic age estimate usually adopted for pulsars is not a reliable indicator of the true age for MSPs (see e.g. Tauris et al. 2012). For the binaries one could also try to use the WD companions cooling age estimates (Hansen & Phinney 1998), but this indicator has large uncertainties as well.

A further possibility, of course, is that the recycling scenario

does not apply to isolated MSPs whose different luminosity distribution would be the consequence of a completely different formation mechanism. If they were born directly as isolated objects, for instance, we could expect that their post-Supernova velocities were in average bigger than that of binary systems; consequently we'd expect that their heights ZZ above the Galactic plane were bigger than for binaries. A KS test on the ZZ distributions of our binary and isolated MSP sample, however, does not support this hypothesis.

To further check the idea of different formation histories being the cause of the different distributions, we also compared the luminosity of isolated and binary MSPs in Globular Clusters. In these dense environments, in fact, isolated MSPs are extremely likely to be created by disruption of already formed MSP binary systems by the close encounter with another star (Phinney & Sigurdsson 1991): therefore, isolated and binary MSPs are expected to have had the same evolution, and thus comparable luminosity distributions. A KS test performed on the Cluster MSPs listed in Bagchi et al. (2011) results in a 88% probability that the two populations are indeed equal, corroborating the idea that a difference in luminosity reflects a difference in evolution.

Given the small number of field MSPs and the uncertainties in the distances, however, the hypotheses discussed above are still quite speculative and the discovery of more isolated MSPs is desirable in order to give statistical strength to any of these theses.

PSR J1832–0836 and PSR J1729–2117 (Thornton et al. in preparation) are the only two isolated MSPs found so far in the HTRU survey and they represent a mere 7% of HTRU MSP discoveries. This small percentage is very different from the $\sim 25\%$ of isolated pulsars previously known in the sample of Galactic field MSPs and it is also significantly smaller than the $\sim 12\%$ of isolated objects present among the MSPs discovered through gamma-ray observations (directly or with follow-up radio observations; Ray et al. 2012) thanks to the LAT instrument (Atwood et al. 2009) on board the *Fermi* satellite. The discrepancy between the Galactic isolated MSPs percentage resulting from blind radio surveys and from the targeted follow up of *Fermi* point sources can be explained by the combination of various effects: the discoveries of unidentified *Fermi* sources and the subsequent detection of radio binary MSPs in targeted searches, are not (or less) affected by orbital smearing of the signal (this is not true for blind searches done directly in gamma-rays; see e.g. Pletsch et al. 2012) or by eclipses; also, the fact that some of the gamma-ray flux detected can, in some cases, arise from off-pulse emission produced by intra-binary shocks could enhance the binary detection rate. Binaries, in summary, are less difficult to find than in a blind search in the radio band. The extremely small percentage of HTRU isolated MSPs, on the other hand, could be explained by a luminosity bias. Because of the higher time and frequency resolution of our survey, we are more sensitive to higher-DM MSPs than previous surveys. This means that we are sampling a deeper volume of the Galaxy, especially towards lower latitudes. If, as the histograms of Figure 2 suggest, isolated MSPs are on average less luminous than MSPs in binary systems, going deeper in the Galaxy means being progressively more sensitive to more luminous populations of objects: far away, dim isolated MSPs are lost, while brighter binary MSPs are discovered also deep into the Galactic plane. If we take into account the discoveries in the intermediate latitude part of our survey (where most of our MSPs have been found so far) we indeed see that the isolated MSPs J1729–2117 (Thornton et al. in preparation) and J1832–0836 are the second and third closest MSPs of our sample. If J1832–0836 were at the average distance of 2.5 kpc of our sample of binaries, its flux density would have been barely

above the survey sensitivity limit (Keith et al. 2010), and below it at the average distance as derived from Taylor & Cordes 1993 distance model. As for J1729–2117, its detection in the survey has been possible only because of scintillation, since its average flux density is below the survey sensitivity. The paucity and the characteristics of the HTRU isolated MSPs, hence, further support the hypothesis that this family of recycled objects is intrinsically less luminous than MSPs in binary systems.

4 SEARCH FOR GAMMA-RAY COUNTERPARTS

Prompted by the fact that, as for the vast majority (all but two) of gamma-ray detected pulsars, our five MSPs have $\dot{E} > 3 \times 10^{33}$ erg s⁻¹ and $\sqrt{\dot{E}/d^2} \gtrsim 10^{-16}$ (erg s⁻¹)^{-1/2} kpc⁻² (except for J1825–0319), we searched for their gamma-ray counterparts in the *Fermi*-LAT data, making use of the precise positions and of the rotational and orbital ephemerides obtained in this work.

No obvious counterpart was found in the LAT 2-year Point Source Catalog (Nolan et al. 2012). We hence folded the gamma-ray data using our timing solutions and the `fermi` plugin (Ray et al. 2011) for `tempo2`, in order to enhance the signal above the background. Two different attempts have been made, one with no energy cutoff and taking event class 2 photons from within 5 degrees of our targets, a second one selecting only photons with energy higher than 300 MeV and using an extraction radius of 1 degree, accounting for the smaller point spread function at higher energies. In both cases we excluded events with zenith angles $> 100^\circ$ to reject atmospheric gamma-rays from the Earth’s limb and we applied the temporal cuts recommended for the galactic point sources in the *Fermi* Science Support Centre web page, through the `gtmktime` tool.

No pulsating counterparts were found folding the entire *Fermi* data set nor folding only the photons in the time span over which the radio timing solution was obtained. This latter attempt was made to account for possible, though unlikely, timing noise or glitching events occurring outside our data span, that would have changed the phase of arrival of gamma ray photons on a longer data set. The lack of detection could be, at least for some of the sources, ascribed to the fact that the real \dot{P} , hence the real \dot{E} of these pulsar is smaller than the observed one (see §2.1). Moreover, using the distance obtained with the Taylor & Cordes (1993) model, brings the $\sqrt{\dot{E}/d^2}$ of four of our MSPs (except J1545–4550) below the limit of 10^{-16} (erg s⁻¹)^{-1/2} kpc⁻² below which only two MSPs have a detected pulsed gamma-ray counterpart.

5 POLARIMETRY OF FOUR MILLISECOND PULSARS

In the following we present the polarisation analysis carried out for four of our five MSPs. No polarisation calibration was possible for the timing observations that we performed with the Lovell telescope; given its peculiar pulse profile and its relative brightness, however, we decided to obtain calibrated polarisation information also for J1832–0836, to try and understand the geometry of its radio beam. We hence observed it with the Parkes radio telescope for ~ 1.5 hr on one occasion. For J1825–0319, on the other hand, getting a good polarisation profile would have required a much longer ($\sim 25\times$) integration time. For this reason, and considering that its single, relatively narrow pulse profile (see Fig 7) would likely lead to a poorly constraining measurement, we decided to discard it from the polarimetric analysis.

To compensate for the different gains of the two feeds, every timing pointing was calibrated using observations of a square wave obtained within $\sim 0.5 - 1$ hour of it. We also calibrated the observations in flux density using observations of Hydra A. Finally we corrected for the variable relative feed orientation across the various parallactic angles.

In order to obtain reliable results from the polarisation analysis, it is necessary to account for the Faraday rotation across our 256 MHz band, hence measuring and correcting for the Rotation Measure (RM). The RM was derived as follows: first we equally divided the total observed bandwidth in four sub-bands for every observation. We then created integrated profiles for the four channels separately, summing all the observations, each properly weighted according to its SNR. For each channel, we obtained an average Polarisation Angle (PA) as in Noutsos et al. (2008):

$$PA_{\text{ave}} = \frac{1}{2} \arctan \left(\frac{\sum_{i=n_{\text{start}}}^{n_{\text{end}}} U_i}{\sum_{i=n_{\text{start}}}^{n_{\text{end}}} Q_i} \right) \quad (1)$$

where n_{start} and n_{end} are the initial and the final bin numbers of the pulse, U_i and Q_i are the two Stokes parameters for the i -th bin. Since we noticed that in J1431–5736 averaging over the entire pulse compromised the quality of the RM fit, we decided to derive the average PAs across the individual components of the summed linearly polarised profiles independently. We then performed a least squares fit to compute the RM:

$$PA_{\text{ave}}(f) = PA_{\text{ref}} + RMc^2 \times \left(\frac{1}{f^2} - \frac{1}{f_{\text{ref}}^2} \right) \quad (2)$$

where $PA_{\text{ave}}(f)$ is the PA_{ave} at a certain frequency f , PA_{ref} is the PA_{ave} at a reference frequency f_{ref} , and c is the speed of light (e.g. Lorimer & Kramer 2005).

As a final step, we corrected the observations for the computed RM and we summed them obtaining the frequency integrated polarisation profiles described in the following subsections. The main polarisation parameters for the four pulsars presented are summarised in Table 4.

Polarisation studies are fundamental to investigate the geometry of pulsars as well as their magnetic fields and radio beam structures. In the ideal case, the interpretation of the results of this kind of analysis could be carried out using the Rotating Vector Model (RVM) by Radhakrishnan & Cooke (1969). This model assumes that the position angle of the linear polarisation ($L = \sqrt{Q^2 + U^2}$) is tied to that of the pulsar magnetic field lines. In this way, its prediction is to observe a swing of the Polarisation Angle (PA) curve across the pulse (that should produce a characteristic “S-shape”), due to the sweeping of the observer’s line of sight through the radio beam.

The fit of the model should permit the inclination between the magnetic and the rotational axes and the impact parameter between the line of sight and the magnetic axis to be obtained.

This however is not always possible, for example because the polarisation signal-to-noise ratio (SNR) is not high enough to allow a good determination of the PA, or the pulse is so narrow that there is not enough information to constrain the fit, or also because the predicted PA swing is not displayed (for a thorough discussion of the difficulties and limitation of the RVM see Everett & Weisberg 2001). MSP PAs, in particular, often display jumps or discontinuities in the PA profile: this is the case of our MSPs, as described below, for which hence a fit using the RVM has not been possible.

Table 4. Rotation measure, linear polarisation, net and absolute circular polarisations (in flux density and in percentage of the total intensity) for the three pulsars timed at Parkes and J1832–0836. The top part of the table refers to measurements obtained at 20 cm, while the second and third, for J1545–4550 only, at 10 cm and 40 cm respectively. The peaks are numbered left to right in the plots, except for the IV peak of J1545–4550, being the left-most at 40 cm. The peaks with two blended components for J1832–0836 (around phases -0.05 and 0.3 in Fig. 5), are computed as a single peak.

Name	RM (rad/m ²)	<i>L</i> (mJy)	<i>L</i> / <i>S</i> (%)	<i>V</i> (mJy)	<i>V</i> / <i>S</i> (%)	<i>V</i> (mJy)	<i>V</i> / <i>S</i> (%)
20-cm							
J1431–5740	-50 ± 15	0.068(3)	19.3(8)	$-0.088(4)$	$-25(1)$	0.092(2)	26.3(8)
J1545–4550	-0.6 ± 1.3	0.299(4)	53.1(4)	$-0.094(2)$	$-16.6(4)$	0.094(1)	16.7(3)
peakII	-6.6 ± 7.8	0.064(1)	100(6)	0.009(2)	15(4)	0.011(1)	17(2)
peakIII	-6.0 ± 1.1	0.074(1)	58(2)	$-0.018(3)$	$-14(2)$	0.018(1)	14(1)
J1832–0836	25 ± 17	0.122(9)	25(2)	0.04(1)	8(3)	0.046(7)	9.7(16)
peakII	–	0.048(5)	16(2)	0.00(1)	0(3)	0.000(4)	0.0(15)
peakIII	–	0.048(7)	18(3)	$-0.023(8)$	$-8(3)$	0.038(5)	14(2)
peakIV	–	0.049(7)	67(12)	0.012(8)	17(12)	0.027(5)	38(8)
J2236–5527	27.8 ± 1.4	0.062(2)	22.1(8)	$-0.001(3)$	0(1)	0.029(2)	10.5(7)
10-cm							
J1545–4550	10.5 ± 5.7	0.121(1)	58(1)	$-0.022(3)$	$-11(1)$	0.022(2)	10.5(8)
peakII	–	0.010(2)	38(7)	$-0.002(2)$	$-8(9)$	0.002(1)	8(5)
40-cm							
J1545–4550	3 ± 15	0.37(2)	35(2)	$-0.17(3)$	$-17(3)$	0.17(2)	17(2)
peakII	-9.7 ± 8.9	0.34(1)	92(5)	0.05(2)	12(6)	0.05(1)	12(3)
peakIII	-0.7 ± 0.6	0.15(1)	100(25)	0.001(23)	1(21)	0.02(1)	14(12)
peakIV	–	0.14(2)	33(5)	0.02(3)	6(8)	0.05(2)	13(5)

5.1 J1431–5740

The pulse profile for J1431–5740 (Fig. 3) shows a single slightly asymmetric peak. The linear polarisation, however, displays two peaks, whereof the leading is fainter and wider in amplitude than the trailing. The minimum of the linear polarisation occurs roughly at the phase of the peak in the total intensity profile. The PAs in correspondence with the leading peak show a slightly decreasing slope, while the PA curve of the trailing component is flat. The two series of PAs exhibit an orthogonal (within the uncertainties) jump in between. The circular polarisation profile shows a single component, whose peak appears in phase with that of the total intensity.

5.2 J1545–4550

This pulse profile at 20 cm (central panel of Figure 4) shows three well defined components: two of them are contiguous, while the third one is 0.22 in rotational phase away from the closest component. A fourth component is barely visible about 0.4 in phase before the main peak. It acquires statistical significance when comparing the 20-cm profile to the 40-cm one (bottom panel of Fig. 4) where this fourth component emerges clearly. The linear polarisation profile follows the total intensity one, and the percentage of *L* under every component is very high, especially beneath the second peak. The PA curve of the component with higher SNR shows a short, steep rise and a smooth decline toward the separation between the first and the second component. A similar smooth decline with almost the same inclination is shown by the PA curve of the third peak, while that of the second one is flatter and exhibits a jump of $\sim 90^\circ$ with respect to the first. The circular polarisation appears mainly under the first component where it is fully negative, while

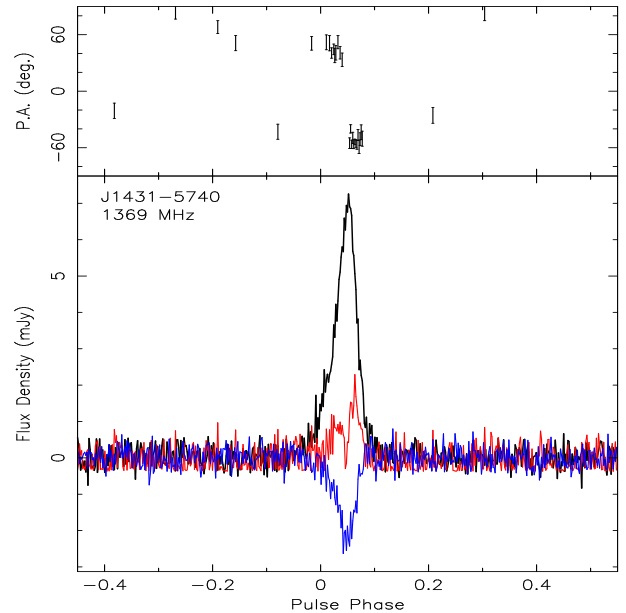


Figure 3. Polarisation profile for J1431–5740 at a centre frequency of 1369 MHz. The lower panel shows, in black, the total intensity, in light grey (red in the electronic version) the linearly polarised intensity *L* and in dark grey (blue in the electronic version) the circularly polarised intensity *V*. The top panel gives the PA of the linearly polarised emission.

there are just hints of circular polarisation beneath the other two peaks, with opposite signs.

As mentioned in §2.1, for this pulsar a few observations at 10 and 40 cm are also available. Given the smaller number of data points, the resulting profiles, especially the one at 40 cm, whose

band is often corrupted by RFI, are not as high S/N as the 20-cm one. At 10 cm (top panel of Figure 4) the first peak appears ~ 35 per cent narrower than at 20 cm and the third peak is statistically undetectable. The linear and circular polarisation profiles of the main peak behave as at 20 cm, while the second peak appears to be unpolarised. The 40-cm profile (bottom panel of Figure 4) shows four components: besides the three clearly present at 20 cm, whose peaks are closer together at this lower frequency, a fourth component precedes in phase the main peak by $1/3$. The percentage of linear polarisation of the main peak drops by about 30 per cent with respect to the 20-cm value, while the second and third peaks appear 100 per cent linearly polarised (even though for the latter, as for the fourth peak, the statistic is quite poor). The circular polarisation is negative below the main peak and positive below the second one. In contrast with what is generally found (Manchester 1971; Xilouris et al. 1996), for this object the percentage of linear polarisation (at least in the main peak where a trend through all three frequencies can be easily seen) decreases with decreasing frequency while the percentage of circular polarisation increases (in absolute value).

The pattern of the PA curves are very similar at the three frequencies and the RM values calculated on the three data sets separately are always compatible with zero at $2\text{-}\sigma$.

5.3 J1832–0836

This MSP shows a complex pulse profile displaying six components (see Fig. 5), two of which are blended with the adjacent one. The polarisation values for the two peaks with the two blended components are computed for both components together in Table 4, listing hence a total of four peaks (centred approximately around phases -0.05 , 0.23 , 0.3 and 0.57). Unfortunately the polarisation is quite small and the PAs do not allow us to clearly understand the beam structure leading to such a peculiar profile. The PAs in correspondence of the two components around phase 0.0 are separated by a jump of almost 100° , with the second component showing a slightly negative slope. In contrast the peaks at phase ~ 0.25 and ~ 0.57 have PAs that appear flatter, with a slightly positive slope for the latter.

The linear polarisation profile shows five peaks, with only the second component of the peak around phase 0.3 apparently unpolarised. We computed an RM value for every linearly polarised peak separately, however, due to the poor signal-to-noise ratio of the polarised emission, the errors are often very high and most of the RMs are compatible with zero at $2\text{-}\sigma$. The RM measured on the peak centred at phase 0.0, the one showing the highest level of polarisation and giving the smallest error is $\text{RM} = 35 \pm 2 \text{ rad/m}^2$. To confirm this value we also measured the RM with the methods described in Noutsos et al. (2008) and in Han et al. (2006), yielding respectively values of $50 \pm 30 \text{ rad/m}^2$ and $25 \pm 17 \text{ rad/m}^2$. Testing these results with a matrix template matching technique, we found out that a value close to 25 rad/m^2 better describes the data.

The circular polarised emission is visible, with changing signs, in correspondence with the peaks at phase ~ 0.0 , ~ 0.3 and ~ 0.57 .

5.4 J2236–5527

The total intensity profile of this MSP (Fig. 6) shows two blended peaks and two additional much fainter components separated in phase from the main one by -0.42 and 0.22 respectively. We considered just the main components, since there is no evidence of

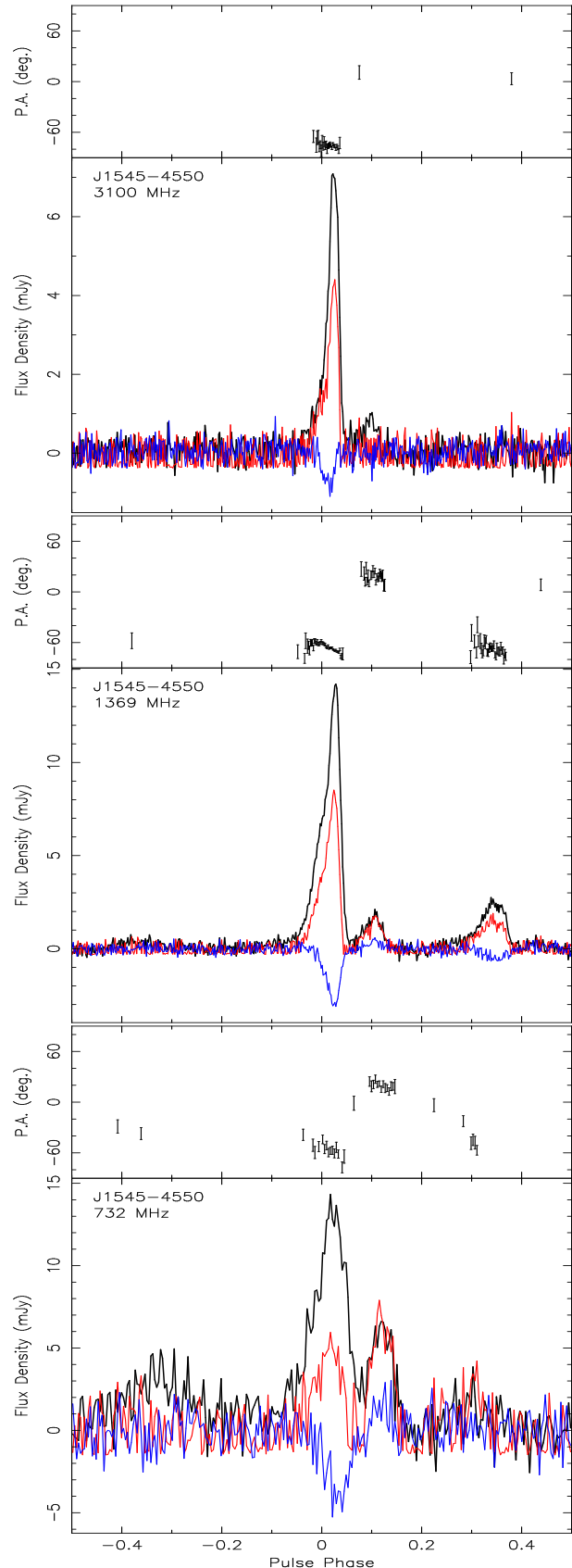


Figure 4. Polarisation profiles for J1545–4550 at centre frequencies of 3100 MHz (top), 1369 MHz (centre) and 732 MHz (bottom). Lines and panels as in Figure 3. The pulses at the different frequencies are aligned so that the centroid of the main peak falls at phase 0.

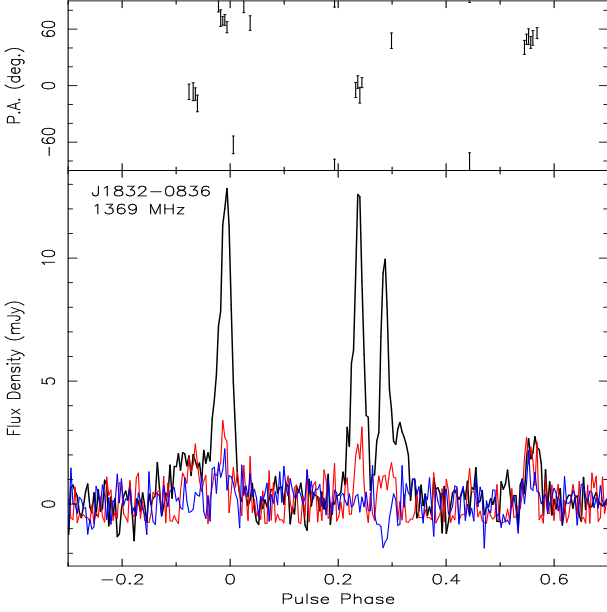


Figure 5. Polarisation profiles for J1832–0836 at a centre frequency of 1369 MHz. Lines and panels as in Figure 3.

polarised signal for the other two. The linear polarisation profile shows three peaks. We computed the RM for each of the peaks separately: the RMs of the first and the third peak seem to be consistent with zero although with a very high uncertainty, while the central peak gives a RM value of $\sim 27.8 \pm 1.3$ rad/m². The PAs of the first component draw a flat curve, and are separated from the PAs related to the second peak by a jump of almost $\sim 100^\circ$. For the central component the PA curve shows a steep decrease, whereas it increases in correspondence with the third component. Circularly polarised emission is present mainly at the same pulse longitude of the second and the third component of the linear polarisation, with a V profile sign change occurring at the same time of the PA's slope change.

6 CONCLUSIONS

In this paper we presented the discovery and timing results of five MSPs detected in the HTRU survey data. Four of them belong to binary systems with He-WD companions, while the fifth is one of the only two isolated MSPs found so far in this survey. A revision of the luminosity distribution of known isolated and binary MSPs is presented; with the sample of isolated MSPs increased by more than 60 per cent and the total sample of MSPs tripled with respect to the previous works addressing this issue (e.g. Lorimer et al. 2007), the intrinsic luminosity difference between these two populations appears to be confirmed. The small percentage of isolated objects among MSP discoveries in the HTRU survey, sampling a deeper volume of the Galaxy with respect to previous experiments, also supports the hypothesis that the intrinsic luminosity difference is indeed real. This effect could be the consequence of a different evolutionary history experienced by isolated and binary MSPs.

For four of our targets, those for which we have follow-up observation carried out at the Parkes radio telescope, we also reported the results of a polarimetric analysis. The possibility to calibrate their polarisation accurately also allowed us to obtain an improved timing solution for two of our MSPs.

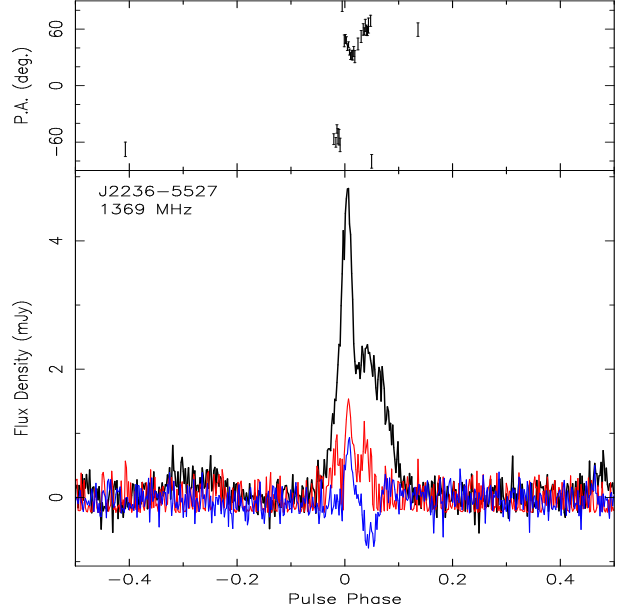


Figure 6. Polarisation profiles for J2236–5527 at a centre frequency of 1369 MHz. Lines and panels as in Figure 3.

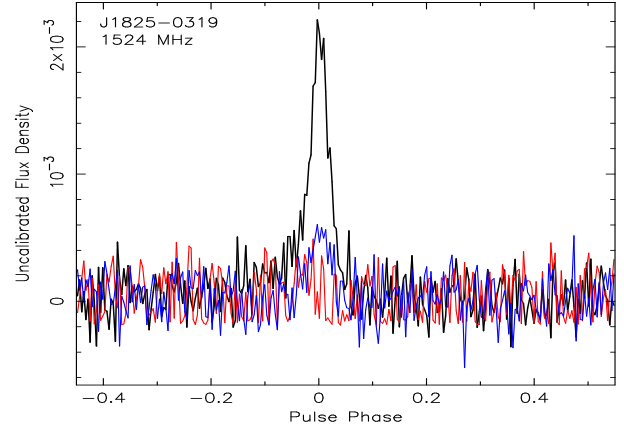


Figure 7. Uncalibrated profile for J1825–0319 at a centre frequency of 1369 MHz. Lines and panels as in Figure 3.

Thanks to the precise ephemerides obtained through radio timing, we could fold in phase the gamma-ray photons collected by the *Fermi*-LAT instrument since its launch from the direction of the MSPs. Unfortunately no pulsating high-energy counterpart to any of our MSPs was found, nor were point sources corresponding to the position of our targets present in the 2-yr *Fermi* Point Source Catalog (Nolan et al. 2012).

One of the main aims of the High Time Resolution Universe Pulsar Survey (Keith et al. 2010) is that of discovering stable millisecond pulsars suitable to be included in pulsar timing array experiments for the detection of gravitational waves (Hellings & Downs 1983). Two of the newly discovered MSPs show quite small timing residuals, which makes them good candidates to be used in pulsar timing arrays: J1545–4550 is indeed the second HTRU MSP to be included in the Parkes PTA and J1832–0836 is being considered for the European and North American PTAs.

7 ACKNOWLEDGEMENTS

The Parkes radio telescope is part of the Australia Telescope which is funded by the Commonwealth of Australia for operation as a National Facility managed by CSIRO.

Part of this research was carried out at the Jet Propulsion Laboratory, California Institute of Technology, under a contract with the National Aeronautics and Space Administration.

MBu and AP have been partly funded under the ASI contract I/047/08/0-WP3000 (Fermi).

REFERENCES

- Alpar M. A., Cheng A. F., Ruderman M. A., Shaham J., 1982, *Nature*, 300, 728
- Atwood W. B., et al. 2009, *ApJ*, 697, 1071
- Bagchi M., Lorimer D. R., Chennamangalam J., 2011, *MNRAS*, 418, 477
- Bailes M., et al., 1997, *ApJ*, 481, 386
- Bailyn C. D., Grindlay J. E., 1990, *ApJ*, 353, 159
- Bates S. D., et al., 2011, *MNRAS*, 416, 2455
- Bhattacharya D., van den Heuvel E. P. J., 1991, *Phys. Rep.*, 203, 1
- Camilo F., et al., 2001, *ApJ*, 548, L187
- Camilo F., Nice D. J., Taylor J. H., 1996, *ApJ*, 461, 812
- Cordes J. M., Lazio T. J. W., 2002 e-print arXiv:astro-ph/020715
- Eatough R. P., Kramer M., Lyne A. G., Keith M. J., 2013, *MNRAS*
- Edwards R. T., Bailes M., 2001, *ApJ*, 553, 801
- Everett J. E., Weisberg J. M., 2001, *ApJ*, 553, 341
- Faulkner A. J., Stairs I. H., Kramer M., Lyne A. G., Hobbs G., Possenti A., Lorimer D. R., Manchester R. N., McLaughlin M. A., D’Amico N., Camilo F., Burgay M., 2004, *MNRAS*, 355, 147
- Ferdman R. D., et al., 2010, *Classical and Quantum Gravity*, 27, 084014
- Han J. L., Manchester R. N., Lyne A. G., Qiao G. J., van Straten W., 2006, *ApJ*, 642, 868
- Hansen B. M. S., Phinney E. S., 1998, *MNRAS*, 294, 557
- Hellings R. W., Downs G. S., 1983, *ApJ*, 265, L39
- Hessels J. W. T., et al., eds, American Institute of Physics Conference Series Vol. 1357 of American Institute of Physics Conference Series, A 350-MHz GBT Survey of 50 Faint Fermi γ -ray Sources for Radio Millisecond Pulsars. pp 40–43
- Hobbs G., Lorimer D. R., Lyne A. G., Kramer M., 2005, *MNRAS*, 360, 974
- Hobbs G. B., Edwards R. T., Manchester R. N., 2006, *MNRAS*, 369, 655
- Hotan A. W., van Straten W., Manchester R. N., 2004, *PASA*, 21, 302
- Janssen G. H., Stappers B. W., Bassa C. G., Cognard I., Kramer M., Theureau G., 2010, *A&A*, 514, A74
- Jenet F., et al., 2009, e-print arXiv:0909.1058
- Keith M. J., et al., 2010, *MNRAS*, 409, 619
- Keith M. J., et al., 2012, *MNRAS*, 419, 1752
- Kluźniak W., Ruderman M., Shaham J., Tavani M., 1988, *Nature*, 334, 225
- Kramer M., et al., 2006, *Science*, 314, 97
- Kramer M., Xilouris K. M., Lorimer D. R., Doroshenko O., Jessner A., Wielebinski R., Wolszczan A., Camilo F., 1998, *ApJ*, 501, 270
- Lommen A. N., Kipporn R. A., Nice D. J., Splaver E. M., Stairs I. H., Backer D. C., 2006, *ApJ*, 642, 1012
- Lorimer D. R., et al., 2006, *MNRAS*, 372, 777
- Lorimer D. R., Kramer M., 2005, *Handbook of Pulsar Astronomy*. Cambridge University Press
- Lorimer D. R., et al., 2004, *MNRAS*, 347, L21
- Lorimer D. R., McLaughlin M. A., Champion D. J., Stairs I. H., 2007, *MNRAS*, 379, 282
- Manchester R. N., 1971, *ApJS*, 23, 283
- Manchester R. N., et al., 2013, accepted by *PASA*, e-print arXiv:1210.6130
- Manchester R. N., Hobbs G. B., Teoh A., Hobbs M., 2005, *AJ*, 129, 1993
- Manchester R. N., et al., 2001, *MNRAS*, 328, 17
- Michel F. C., 1987, *Nature*, 329, 310
- Morris D. J., et al., 2002, *MNRAS*, 335, 275
- Nolan P. L., et al. 2012, *ApJS*, 199, 31
- Noutsos A., Johnston S., Kramer M., Karastergiou A., 2008, *MNRAS*, 386, 1881
- Phinney E. S., 1992, *Philos. Trans. Roy. Soc. London A*, 341, 39
- Phinney E. S., Evans C. R., Blandford R. D., Kulkarni S. R., 1988, *Nature*, 333, 832
- Phinney E. S., Kulkarni S. R., 1994, *Ann. Rev. Astr. Ap.*, 32, 591
- Phinney E. S., Sigurdsson S., 1991, *Nature*, 349, 220
- Pletsch H. J., et al., 2012, *Science*, 338, 1314
- Press W. H., Flannery B. P., Teukolsky S. A., Vetterling W. T., 1986, *Numerical Recipes: The Art of Scientific Computing*. Cambridge University Press, Cambridge
- Radhakrishnan V., Cooke D. J., 1969, *Astrophys. Lett.*, 3, 225
- Ransom S. M., Eikenberry S. S., Middleditch J., 2002, *AJ*, 124, 1788
- Ransom S. M., et al., 2011, *ApJ*, 727, L16
- Ray P. S., et al., 2012, proceedings of the 2011 Fermi Symposium, e-print arXiv:1205.3089
- Ray P. S., et al., 2011, *ApJS*, 194, 17
- Ray P. S., et al., 2013, *ApJ*, 763, L13
- Roy J., Bhattacharyya B., Gupta Y., 2012, *MNRAS*, 427, L90
- Schnitzeler D. H. F. M., 2012, *MNRAS*, 427, 664
- Shklovskii I. S., 1970, *Sov. Astron.*, 13, 562
- Stairs I. H., Thorsett S. E., Taylor J. H., Wolszczan A., 2002, *ApJ*, 581, 501
- Stappers B. W., et al., 1996, *ApJ*, 465, L119
- Tauris T. M., Langer N., Kramer M., 2012, *MNRAS*, 425, 1601
- Taylor J. H., Cordes J. M., 1993, *ApJ*, 411, 674
- van den Heuvel E. P. J., van Paradijs J., 1988, *Nature*, 334, 227
- van Straten W., Bailes M., 2011, *PASA*, 28, 1
- Weisberg J. M., Nice D. J., Taylor J. H., 2010, *ApJ*, 722, 1030
- Wex N., 1998, *MNRAS*, 298, 67
- Xilouris K. M., Kramer M., Jessner A., Wielebinski R., Timofeev M., 1996, *A&A*, 309, 481

This paper has been typeset from a \LaTeX file prepared by the author.